Available online www.jocpr.com

Journal of Chemical and Pharmaceutical Research, 2014, 6(6):2346-2352

Research Article

ISSN : 0975-7384
CODEN(USA) : JCPRC5

Research on local plastic strain at crack tip of dissimilar weld joints in nuclear power plant

Lingyan Zhao[1], He Xue[2] and Zhenwen Wang

[1]School of Science, Xi'an University of Science and Technology, Xi'an, PR China
[2]School of Mechanical Engineering, Xi'an University of Science and Technology, Xi'an, PR China

---

ABSTRACT

The material and grain boundary properties of dissimilar weld joints in nuclear power plant are quite different with homogenous material. The narrow zone near fusion boundary (FB) has been found to have the highest residual strain and hardness, which makes dissimilar weld joints more susceptible to stress corrosion cracking (SCC). Limited experimental conditions, varied influence factors and diverging experimental data make it difficult to accurately predict the SCC behavior of dissimilar weld joints. To clarify the effect of sampling location on SCC driving force such as for cracking in an Alloy 182-low alloy steel dissimilar weld joint, a more reasonable material model with inhomogeneous mechanical property, performed by finite element codes, is applied to simulate the complex mechanical properties of material around FB line. When growing crack enters into the high hardness zone (HHZ) near FB line, the crack driving force decreases quickly. The HHZ is expected to be a serious barrier to further SCC crack growth into low alloy steel (LAS). Potential path for crack growing is also discussed.

Key words: Mechanical heterogeneity, SCC, Sampling location, Crack driving force, HHZ

INTRODUCTION

As a weld filler metal, Alloy 182 are widely used in joining the low alloy steel (LAS) reactor pressure vessel (RPV) and pressure vessel nozzles to austenitic stainless steels. Failures of dissimilar weld joints between the pressure vessel nozzle and main pipe in nuclear power plant have shown that Ni-based alloy and its associated weld metals are more susceptible to stress corrosion cracking (SCC) in simulated high temperature water environments of light water reactor (LWR) [1, 2]. The higher high-temperature yield strength of Alloy 182 makes it more susceptible to SCC and produce high weld residual stresses [3]. Besides cold work and sensitization, the complex crystallographic structures, increased strength and high residual strain adjacent to the fusion boundary (FB) are identified crucial for SCC growth behavior of Alloy 182-LAS dissimilar weld joints in LWR. Recent research revealed that the narrow zone near FB had the highest residual strain and hardness in weld region [4, 5]. The positive hardness gradient of the high hardness zone (HHZ) adjacent to FB in Alloy 182 could lead to a decreased crack growth rate towards LAS [6]. A great deal of evidence and experiments indicated that the material plasticity and residual plastic strain also have great effect on SCC growth rate [7, 8], but its SCC mechanism is still unclear.

In previous fracture research, a weld joint was usually simplified as a sandwich-like configuration including the base metal (BM), the weld metal (WM) and the heat effect zone (HAZ). It is almost impossible to predict SCC growth rate around the FB line because of the discontinuous material mechanical parameters. To investigate the effect of high hardness and residual strain of FB region in an Alloy 182-A533B LAS dissimilar weld joint on its SCC behavior, a detailed material model considering the inhomogeneous mechanical property of a dissimilar weld joint was applied. Under the same load K_I, the local stress-strain fields ahead of propagating crack tips were calculated by using elastic-plastic finite element method (EPFEM). Moreover, the effect of sampling location on plastic strain, plastic zone and SCC driving force in the stationary and growing crack tips of a dissimilar weld joint were analyzed.

Potential path for crack growing was also discussed in this paper.

1. CALCULATION MODEL

2.1 Geometric model

A compact tension (CT) specimen with a constant load K_I was used to measure SCC growth rate in high temperature water environment [8]. Since the width of the narrow zone near fusion line in the HAZ was supposed to be about 100μm [6], the environmental assisted cracking (EAC) numerical tests with three 0.25T-CT specimens were performed to investigate the effect of sampling location on SCC growth rate in an Alloy 182-A533B dissimilar weld joint. This numerical simulation process was guided by American Society for Testing and Materials (ASTM) standards [9]. Geometric shape and size of 0.25T-CT specimen are shown in Fig. 1.

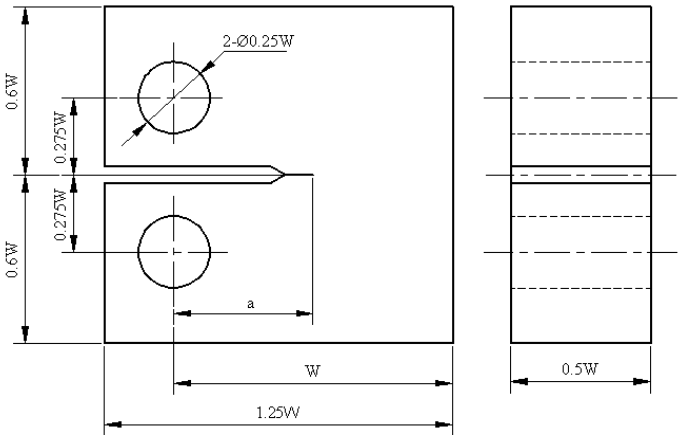

Fig. 1: Geometric shape and size of the 0.25T-CT specimen (where W=12.5mm, a=0.5W)

Fig. 2 shows the sampling location in an Alloy 182-A533B dissimilar weld joint. Three specimens are named FB specimen, WM specimen and transition zone (TZ) specimen, respectively. Since the yield strength of the alloy 82/182 fusion weld metal at the bottom is 50-70MPa higher than that at the top [10], three specimens are all located in the same horizontal line to be sure that the material mechanical properties keep consistent. The focus is the narrow zone called HHZ, whose width is supposed to be 100μm. The crack in FB specimen propagates from the dilution zone (DZ) in Alloy 182, then across the HHZ and finally enters into the HAZ in LAS; the crack in WM specimen propagates in Alloy 182; the crack in TZ specimen propagates from the TZ to 316L. And the crack advanced length (a) is 0.2mm.

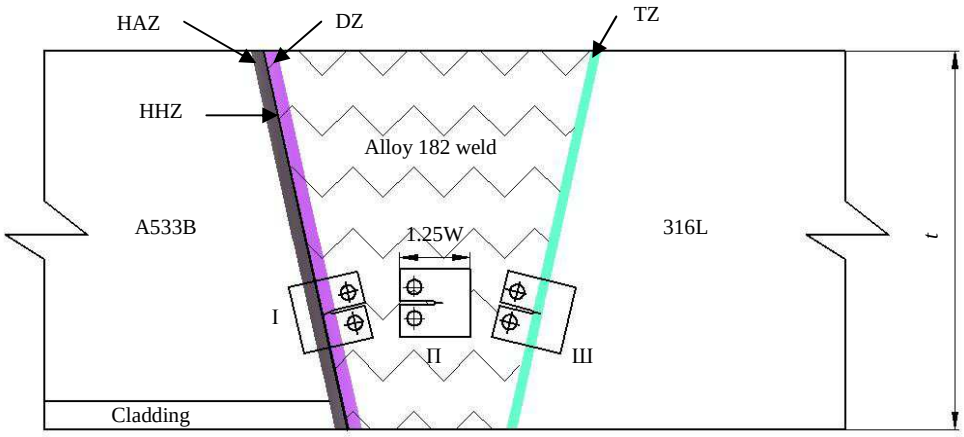

Fig. 2: Schematic diagram of the sampling position in an Alloy 182-A533B LAS dissimilar weld joint (where Ⅰ-FB specimen, Ⅱ-WM specimen, Ⅲ-TZ specimen)

2.2 Material model

Continuously changing mechanical properties of the DZ, HHZ and HAZ is the key point in this simulation, which comes from the material micro-hardness measurement. At first, a linear conversion formula between hardness and yield stress was established. Then the yield stress equations, including one curve in the HHZ and two lines in the DZ and HAZ, were constructed according to the dependence with X position. Fig. 3 delineates the changing yield stress of the DZ, HHZ and HAZ in FB specimen. The mechanical relationship represented by Ramberg-Osgood equation

can be written as

$$\frac{\varepsilon}{\varepsilon_0}=\frac{\sigma}{\sigma_0}+\alpha(\frac{\sigma}{\sigma_0})^n \quad (1)$$

The strain-hardening exponents with different yield strengths are estimated [11]:

$$n=\frac{1}{\kappa\ln(1390/\sigma_0)} \quad (2)$$

Where, κ= 0.163.

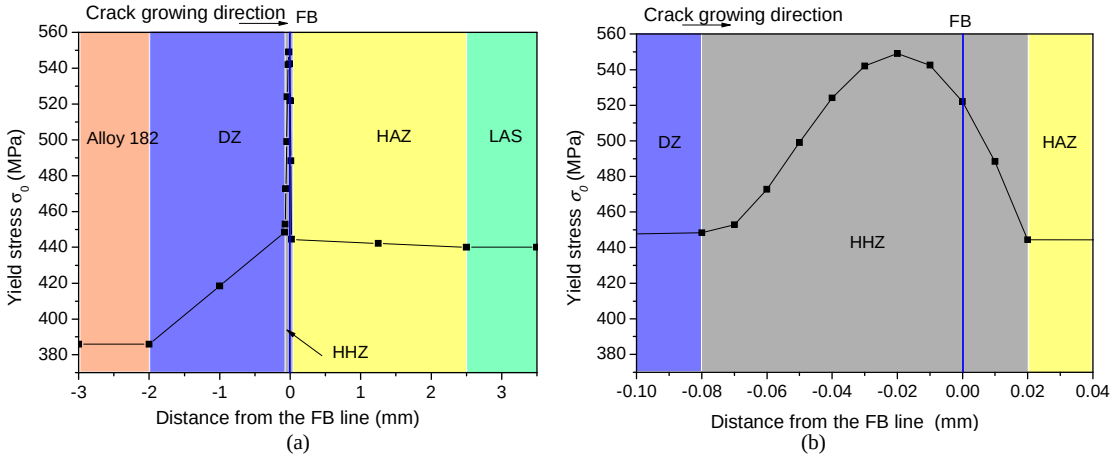

Fig. 3: Yield stress distribution of the FB specimen near the HHZ (a) and yield stress distribution near the FB (b)

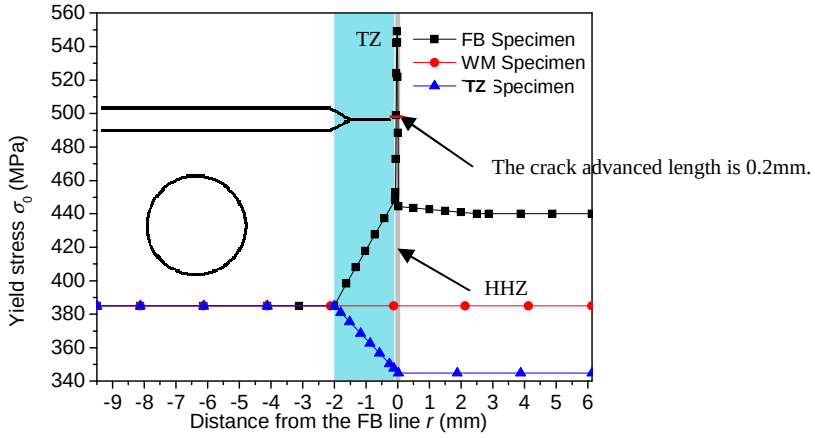

Fig. 4: Yield stress distribution of three 0.25T-CT specimens

Table.1: Material mechanical parameters for the FEM simulation

Material	Young's modulus E (GPa)	Poison ratio ν	Yield stress σ_0 (MPa)	Hardening exponent n	Constant α
LAS (A533B)	189.5	0.288	440	5.333	1.0
DZ					
HHZ	193	0.288	---	---	1.0
HAZ					
Alloy 182	193	0.288	385	4.779	1.0
TZ	193	0.288	--	---	1.0
316L	171.4	0.288	345	4.402	1.0

The inhomogeneous mechanical properties of three 0.25T-CT specimens are shown in Fig. 4. The yield stress of WM specimen is a constant value. The yield stress of TZ region is changing along a straight line in TZ specimen. Stress ahead of growing crack tip will be released with larger crack length. All materials listed in Table 1 have the loading and unloading stress-strain relation. Additionally, the material unloading curve is different from its loading curve, which is the main reason to produce different stress-strain fields at the tip of stationary crack and stable

growing crack.

2.3 Finite element model

A commercial FEM code ABAQUS is used in this simulated analysis. With different sampling location, three models were calculated based on the basic loading parameter of stress intensity factor K_I. The constant K_I of 20 MPa·$m^{1/2}$ was adopted in this EAC experiment of simulated LWR environments [7].

Fig. 5 gives the mesh of the global specimen and sub-model specimen, where X-axis is the opposite direction of crack growth and Y-axis is the normal direction of crack. 6697 and 12284 8-node biquadrate plane strain quadrilateral elements was adopted in the global model and sub-model, respectively. Mesh at the vicinity of crack tip is observably refined in both global model and sub-model. Boundaries of sub-model were driven by the stress-strain obtained from the global model analysis.

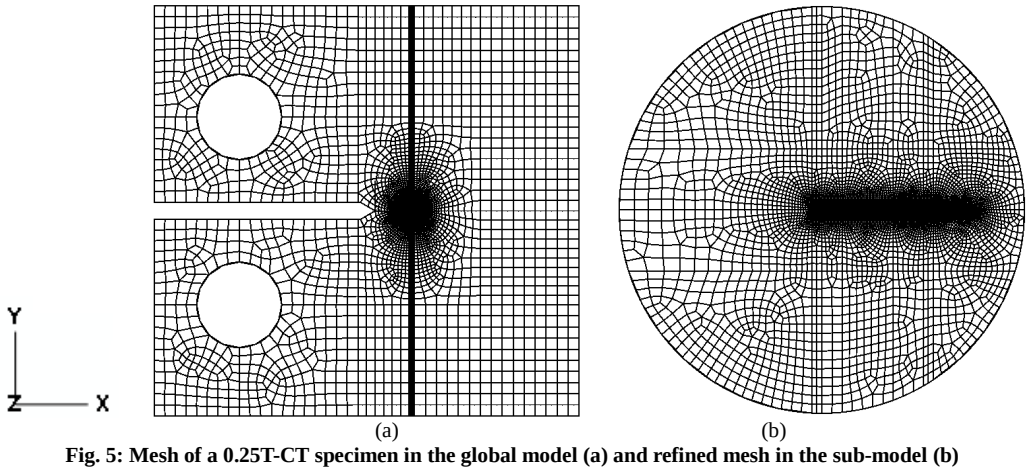

(a) (b)

Fig. 5: Mesh of a 0.25T-CT specimen in the global model (a) and refined mesh in the sub-model (b)

RESULTS AND DISCUSSION

Mechanical affecting factors of crack driving force, such as plastic zone, plastic strain and plastic strain rate ahead of crack tips are crucial to quantitatively predict SCC growth rate. Therefore, in both stationary and growing crack tips of three 0.25T-CT specimens, the local plastic strain and plastic strain rate were investigated in this study.

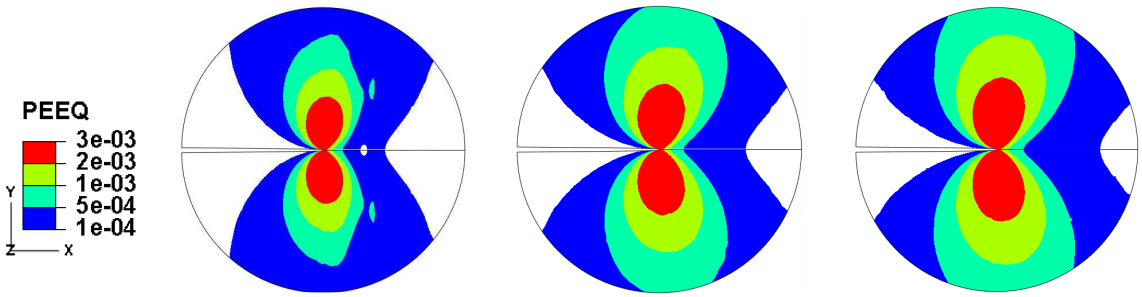

(a) (b) (c)

Fig. 6: Equivalent plastic strain ahead of stationary crack tips in FB specimen (a), in WM specimen (b) and in TZ specimen (c)

3.1. Contours of strain ahead of stationary crack tips

A circular area with 0.4 mm radius around the crack tip was analyzed in the following numerical simulations. Fig. 6 exhibits the equivalent plastic strain ahead of the stationary crack tips when crack begins to propagate. The equivalent plastic strain contours are from 0.0001 to 0.003 in Fig. 6. The equivalent plastic strain ahead of FB specimen's stationary crack tip is lower than other specimens. Whereas, the strain of TZ specimen is higher than that of other specimens, which is caused by lower hardness and yield stress of the material around crack tip.

3.2. Plastic strain of growing crack tips

The normal plastic strain distribution of growing crack tips in FB specimen is shown in Fig. 7, where the plastic strain contours are from 0 to 0.006. Comparing Fig. 7(a) with Fig. 6(a), the plastic strain distributions at growing

crack tip are much smaller than that of stationary crack tip. The reason why is that crack growing can induce an unloading process of stress at crack tip. Under the same loading condition, the plastic strain remains very big near FB specimen crack tip as crack length increases because of the residual plastic strain that induced by the material's unloading curve. Moreover, the plastic strain ahead of propagating crack tips decreases when crack enters into HHZ with higher yield stress.

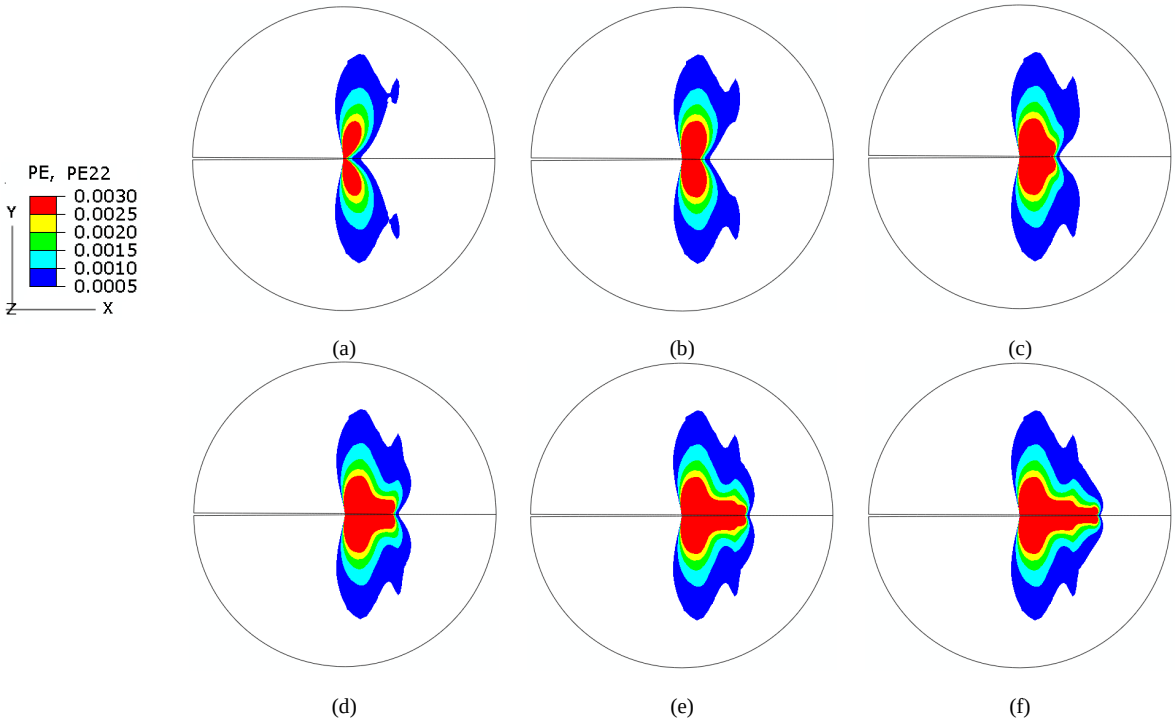

Fig. 7: Normal plastic strain distribution of growing crack tips in FB specimen when Δa=0μm (a), Δa=40μm (b), Δa=80μm (c), Δa=120μm (d), Δa=160μm (e) and Δa=200μm (f)

Fig. 8 shows normal plastic strain curves ahead of growing crack tips at different sample location. All the strains decrease as the crack length increases and finally their values are almost equal. The gray area represents HHZ region in FB specimen. HHZ is not painted in Figs. 8(e) and (f) because growing crack tip of FB specimen has stepped over HHZ. This result indicates that the effect of sample location on growing crack of an Alloy 182-A533B LAS dissimilar weld joint will decrease and finally diminish as crack length increases. In Figs. 8(a), (b) and (c), at the beginning of crack propagation (Δa=0-80μm), there is a bigger gradient of normal plastic strain in FB specimen than that in other specimens, which is caused by the growing crack tip located HHZ with higher yield stress. In Figs. 8(d), (e) and (f), the normal plastic strain gradients are similar among all the specimens when crack finally traverses the HHZ.

Crack tip strain is the main mechanical parameter affecting crack driving force and SCC growth rate in the film degradation/oxidation model. Because it is difficult to obtain crack tip strain directly, plastic strain was used to replace crack tip strain at a characteristic distance r_0 ahead of crack tip when SCC growth rate are calculated [12]. Comparing the crack tip plastic zones where the equivalent plastic strain is 0.2% with different sampling location, the reasonable distance from growing crack tip was designated as 30μm. In Fig. 9, at a characteristic distance (r_0=30μm) from the growing crack tip, the normal plastic strain of FB specimen is observably smaller than that of BM and TZ specimen when the crack length is quite small. These results indicate that normal plastic strain in FB specimen has a larger strain gradient than that of others because the crack crosses the HHZ region where the material yield strength increases. It means that the crack would stop extension in the HHZ zone. Viewed from the mechanical point, because of its highest hardness and residual plastic strain, the FB line in HHZ should be a barrier to the crack in Alloy 182 weld metal extending to LAS.

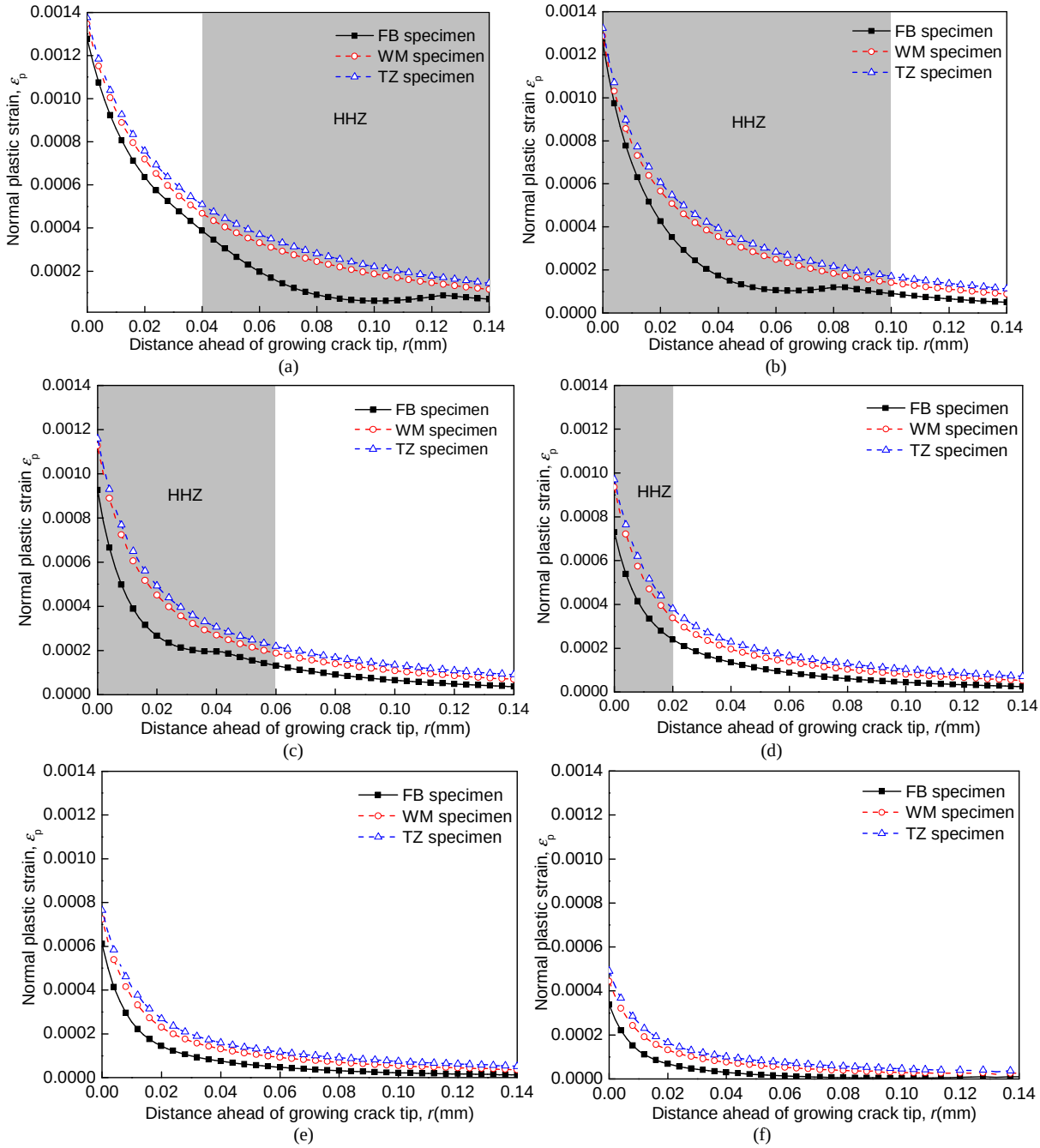

Fig. 8: Normal plastic strain distribution of growing crack tips in FB specimen when Δa=0 μm (a), Δa=40 μm (b), Δa=80 μm (c), Δa=120 μm (d), Δa=160 μm (e) and Δa=200 μm (f)

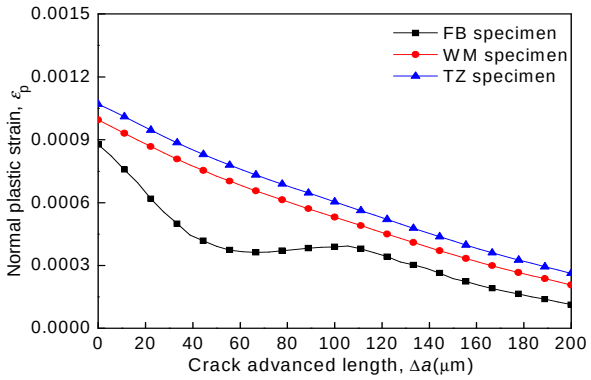

Fig. 9: Normal plastic strains at a characteristic distance from the growing crack tips (r_0=30μm)

CONCLUSION

To analyze the potential path for SCC crack growing, numerical simulations are carried out to analyze the strain and plastic strain rate ahead of growing crack tips. The effect of sample location on crack driving force is also considered. The plastic strain at stationary crack tip is much bigger than that of growing crack tip. The reason why is that unloading process occurs at growing crack tip. Under the same loading condition, as crack length increases, the plastic strain remains very high near the crack tip of FB specimen because of the residual plastic strain. When the crack propagates from the DZ in Alloy 182 towards the FB line, a retardation of the crack growth occurs as the result of a decreased plastic strain rate in residual plastic strain zone. Particularly, the growing crack will stop extension into LAS when it enters into HHZ near the FB line. Viewed from the mechanical point excluding the effect of residual stress, because of its highest hardness and residual plastic strain, the FB line in HHZ should be a barrier to further SCC crack growth into LAS.

Acknowledgments
The authors wish to thank the Natural Science Foundation of China for contract 11072191 and Scientific Research Program Funded by Shanxi Provincial Education Commission for contract 12JK0657, under which the present work was possible.

REFERENCES

[1] Peng Q.J., Hou J., Takeda Y., Shoji T. *Corrosion Science*, v 67, pp. 91-99, **2013**.
[2] Peng Q.J., Xue H., Hou J., Sakaguchi K., Takeda Y. *Corrosion Science*, v 53, n 12, pp. 4309-4317, **2011**.
[3] Andresen P.L., Young L.M., Emigh P.W., Horn R.M. *NACE Corrosion*, CD-ROM, Paper No. 02510, **2002**.
[4] Hou J., Peng Q. J., Takeda Y., Kuniya J., Shoji T. *Corrosion Science*, v 52, n 12, pp. 3949-3954, **2010**.
[5] Hou J., Shoji T., Lu Zh.P., Peng Q.J. *Journal of Nuclear Materials* , v 397, n 1-3, pp. 109-115, **2010**.
[6] Seifert H.P., Ritter S., Shoji T., Peng Q.J. *Journal of Nuclear Materials*, v 378, n 2, pp. 197-210, **2008**.
[7] Xue H., Li Z.J., Lu Z.P., Shoji T. *Nuclear Engineering and Design*, v 241, n 3, pp. 731-738, **2011**.
[8] Xue H., Ogawa K., Shoji T. *Nuclear Engineering and Design*, v 239, n 4, pp. 628-640, **2009**.
[9] ASTM Standard E399-90, *Annual book of ASTM Standards*, v 03.01, ASTM International, **2002**.
[10] Jang Ch.H., Lee J.H., Kim J.S., Jin T.E. International Journal of Pressure Vessels and Piping ,v 85, n 9, pp. 635-646, **2008**.
[11] Ueda Y., Shi Y., Sun S. *Transactions of JWRI*, v 26, n 2, pp. 133-140, **1997**.
[12] Xue H., Sato Y., Shoji T. *Transactions of the ASME-Journal of Pressure Vessel and Technology*, v 131, n 1, pp. 61-70, **2009**.